# Innervation of the Heart: Imaging Findings Using [$^{123}$I]-MIBG Scintigraphy in Different Pathologies

4

Denis Agostini, Kenichi Nakajima and Hein Jan Verberne

## 4.1 Introduction

The heart is innervated by the autonomic nervous system (ANS). The ANS provides innervation through fibers originating from autonomic ganglia located outside the central nervous system (CNS) in response to the preganglionic cholinergic stimulation coming from the CNS. The ANS has great influence on cardiovascular physiology by controlling the cardiac performance (contractility, conduction, and heart rate) to respond quickly and effectively to changing demands. The sympathetic nervous system (SNS) is dominant in the heart, principally in the ventricles.

### 4.1.1 Sympathetic Innervation

The SNS is one of the neurohormonal compensation mechanisms that play key roles in the pathogenesis of heart failure (HF). The SNS, together with the hypothalamic–pituitary–adrenal axis, was thought to play an important supportive role in the flight, fright, and fight reaction of humans and animals in response to stressful situations. The cardiac autonomic nervous system (ANS) consists of two distinct and counteracting forms: sympathetic and parasympathetic innervation. They differ in their major neurotransmitters, norepinephrine and acetylcholine, and exert stimulating or inhibitory effects on target tissues via adrenergic and muscarinic receptors. Both are responsible for electrophysiologic and hemodynamic adaptation of the cardiovascular system to changing demands.

#### 4.1.1.1 Anatomy and Physiology of the SNS in the Myocardium

Whereas parasympathetic fibers are mainly present in the atria and less abundant in ventricular myocardium, the SNS is the predominant autonomic component in the ventricles. Sympathetic fibers travel along epicardial vascular structures and penetrate into underlying myocardium similar to coronary vessels. On the basis of tissue norepinephrine content, the heart is characterized by dense sympathetic innervation with a gradient from the atria to the base of the heart and from the base to the apex of the ventricles [1, 2].

D. Agostini (✉)
Nuclear Medicine, University Hospital CHU, Caen, France
e-mail: agostini-de@chu-caen.fr

K. Nakajima
Department of Nuclear Medicine, Kanazawa University Hospital, Kanazawa, Japan
e-mail: nakajima@med.kanazawa-u.ac.jp

H. J. Verberne
Department of Nuclear Medicine, Amsterdam Medical Center, University of Amsterdam, Amsterdam, The Netherlands
e-mail: h.j.verberne@amc.uva.nl

P. Marzullo and G. Mariani (eds.), *From Basic Cardiac Imaging to Image Fusion*,
DOI: 10.1007/978-88-470-2760-2_4, © Springer-Verlag Italia 2013

#### 4.1.1.2 SNS Neurotransmitters

The dominant sympathetic transmitter, norepinephrine, is synthesized within neurons by an enzymatic cascade. Dihydroxyphenylalanine (DOPA) is generated from tyrosine and subsequently converted to dopamine by DOPA decarboxylase. Dopamine is transported into storage vesicles by the energy-requiring vesicular monoamine transporter. Norepinephrine is synthesized by dopamine $\beta$-hydroxylase within these vesicles. Neuronal stimulation leads to norepinephrine release through fusion of vesicles with the neuronal membrane (exocytosis). Apart from neuronal stimulation, release is also regulated by a number of presynaptic receptor systems, including $\alpha_2$-adrenergic receptors, which provide negative feedback for exocytosis. Apart from norepinephrine, sympathetic varicosities store neuropeptide Y (NPY), methionine enkephalin, leucine enkephalin, $\beta$-endorphin, and adenosine triphosphate (ATP) in small and large vesicles. These neurotransmitters are co-released. It is important to realize that norepinephrine and ATP are locally recycled, whereas peptide neurotransmitters are transported along the sympathetic axon to the nerve terminal. At a high stimulation frequency over a longer period of time, the sympathetic nerve terminal is devoid of peptide neurotransmitters in relation to norepinephrine and ATP. The marked preferential increase in the release of cardiac norepinephrine probably contributes to the eventual depletion of norepinephrine in the failing heart. The heart is also thought to be functionally denervated, with reduction of tyrosine hydroxylase activity to account for the loss of norepinephrine.

In the synaptic cleft, only a small amount of released norepinephrine is actually available to activate postsynaptic receptors on the myocyte surface. Most norepinephrine undergoes reuptake into nerve terminals by the presynaptic norepinephrine transporter (uptake 1 mechanism) and recycles into vesicles or is metabolized in cytosol by monoamine oxidase (MAO). Small fractions of the released norepinephrine diffuse into vascular space, where it can be measured as norepinephrine spillover in coronary sinus or will be taken up by extraneuronal cells via the uptake 2 mechanism and followed by degradation to norepinephrine metabolites by catechol O-methyltransferase (COMT).

Sympathetic neurotransmission is achieved by norepinephrine-mediated activation of postsynaptic adrenoceptors. These are membrane-bound proteins on target tissue and are classified in subtypes according to their molecular biological and pharmacological characteristics. $\beta$-adrenoceptors are highly abundant in the myocardium and exert chronotropic, dromotropic, and inotropic effects. Both $\beta_1$- and $\beta_2$-subtypes are present at a ratio of $\sim$5:1 in the healthy human heart. $\beta_1$-adrenoreceptor activation leads to a much higher degree of adenyl cyclase stimulation compared with $\beta_2$-adrenoreceptor activation. However, the degree of stimulation of muscle contraction is similar for $\beta_1$- and $\beta_2$-adrenoreceptors and is directly related to their relative densities. The $\alpha$-adrenoceptors are mainly present in the vascular wall but are also present in myocardium, where they account for approximately 15% of cardiac adrenergic receptors. Two classes of $\alpha$- adrenergic receptors have been identified: $\alpha_1$ and $\alpha_2$. The $\alpha_1$-adrenergic receptors can be further characterized into various subtypes, which are the result of separate gene products differing in structure, G-protein coupling, tissue distribution, signaling, regulation, and functions. Major arteries (including aorta, pulmonary arteries, mesenteric vessels, and coronary arteries) are heavily populated with $\alpha_1$-receptors, and activation of these receptors by endogenous agonists of $\alpha$-adrenergic receptors, epinephrine, and norepinephrine has been demonstrated to be a major contributor in the regulation of blood flow by vasoconstriction. The $\alpha_2$-adrenergic receptors play a prominent role in SNS regulation. Activation of $\alpha_2$-adrenergic receptors in the brainstem leads to reduced sympathetic tone, with a resultant decrease in heart rate and blood pressure. This effect is augmented by stimulation of $\alpha_2$-adrenergic receptors on sympathetic nerve terminals. These presynaptic $\alpha_2$-adrenergic

receptors serve as autoreceptors regulating catecholamine release. There are three $\alpha_2$-adrenergic receptors subtypes ($\alpha_{2A}$, $\alpha_{2B}$, and $\alpha_{2C}$), and studies using gene-targeting strategies indicate independent functions for each.

In conclusion, $\alpha_2$-adrenergic receptors play an important role in regulating the SNS both centrally, by regulating sympathetic tone, and peripherally, by regulating transmitter release from presynaptic nerve terminals.

#### 4.1.1.3 Uptake 1 and Uptake 2

Reuptake of catecholamines from the synaptic cleft is mediated by high-affinity, low-capacity, sodium-chloride-dependent transporters present in the outer membrane of the presynaptic nerve endings. This transport system is also known as the uptake 1 mechanism and consists of the norepinephrine transporter (NET) and the dopamine transporter (DAT). In addition to uptake 1, catecholamines are removed from the circulation by a second transport system. This second transport system consists of sodium-chloride-independent, corticosterone-sensitive, high-capacity extraneuronal monoamine transporters (EMT) originally discovered as a transport mechanism in rat heart and designated as uptake 2 mechanism. Molecular cloning has shown that uptake 1 and uptake 2 belong to two different families of transporters. The presynaptic neuronal uptake 1 transporters for norepinephrine and dopamine are both members of the solute carrier family of transporters (SLC6A2 and SLC6A3, respectively). Uptake-2 belongs to another subgroup of the SLC transporters (SLC22) and can be placed in the family of organic cation transporters (OCT), which has several members (OCT1, OCT2, and OCT3, or SLC22A1, SLC22A2, and SLC22A, respectively). The classical uptake 2 or EMT is most likely to be represented by OCT3 and is expressed in different organs (i.e., heart, liver, skeletal muscle, placenta, and kidney). OCTs are involved in absorption, distribution, and elimination of endogenous compounds (i.e., amines) as well as of drugs, toxins, and other xenobiotics.

Neuronal reuptake by uptake 1 is quantitatively most important for the clearance of released catecholamines, accounting for ~90% of their removal at the presynaptic nerve endings. Although OCT3 has been proposed to be the classical EMT, the three OCTs together are thought to be responsible for the extra-neuronal clearance of catecholamines that have escaped from reuptake by uptake 1. In general, uptake 1 and uptake 2 mechanisms are thought to have similar functions between species. However, small differences in the relative expression of these mechanisms between species have been reported. Due to these differences in distribution (i.e., expression) of uptake mechanisms, results found in experimental animal studies may not exactly reflect the situation in humans.

#### 4.1.1.4 The SNS and Heart Failure

The SNS is one of the neurohormonal compensation mechanisms that play key roles in the pathogenesis of cardiac heart failure (CHF). Neurohormonal activation and a hyperadrenergic state cause desensitization and down-regulation of cardiac $\beta$-adrenoceptors and alterations in the postsynaptic signal transduction, which further impair myocardial performance. In the failing heart, not only are postsynaptic changes observed but so are presynaptic changes. An impaired cardiac uptake 1 mechanism has been observed. Although the pathogenetic mechanisms for altered presynaptic innervation are not fully elucidated, it is likely that it is by these mechanisms that the high concentration of catecholamines in the synaptic cleft is maintained. These effects probably further sustain and exacerbate the remodeling process [3].

### 4.1.2 From Guanethidine to Meta-Iodobenzylguanidine

#### 4.1.2.1 Guanethidine

In the 1960s, guanethidine, a false neurotransmitter, was found to be a sympathetic selective and potent neuron blocking agent and was

developed as an antihypertensive drug. Guanethidine acts on the presynaptic sympathetic nerve ending by inhibiting or interfering with the release and/or distribution of norepinephrine rather than acting on the postsynaptic (i.e. effector) cell by inhibiting the association of norepinephrine with its receptors. In contrast to ganglionic blocking agents, guanethidine suppresses responses mediated by $\alpha$- and $\beta$-adrenergic receptors equally, but does not produce parasympathetic blockade. Side effects are related to its neuron-blocking properties and include orthostatic and exercise hypotension, sexual dysfunction, and diarrhea. Guanethidine is no longer available in the USA due to its side effects and because there are substantially better drugs available. It is still licensed in some countries, i.e., the UK, for rapid control of blood pressure in a hypertensive emergency.

#### 4.1.2.2 [$^{123}$I]-Meta-Iodobenzylguanidine

The modification of guanethidine into meta-iodobenzylguanidine (MIBG) increased the affinity for the presynaptic sympathetic nerve endings. MIBG labeling with radioactive iodine enabled scintigraphic visualization of presynaptic sympathetic nerve endings in humans. The first clinical application of the radiolabeled [$^{131}$I]-MIBG was visualization of the adrenal medulla and different neural-crest-derived tumors, such as pheochromocytomas and neuroblastomas. The striking myocardial uptake, however, prompted Wieland et al. to suggest the potential use of the radiolabeled MIBG for myocardial imaging [4]. However, due to the suboptimal imaging characteristics of $^{131}$I and a less favorable radiation burden, radiolabeling of MIBG with $^{123}$I for diagnostic scintigraphic purposes was to be preferred. In 1981, Kline et al. [5] were one of the first to report on the use of myocardial scintigraphy with [$^{123}$I]-MIBG in five healthy individuals. They concluded that [$^{123}$I]-MIBG had the potential to provide (semi-) quantitative information on myocardial catecholamine content.

Much work has been done to elucidate the uptake mechanisms of MIBG in the presynaptic sympathetic nerve endings. MIBG localizes in adrenergic nerve terminals primarily via the uptake 1 mechanism (see "Uptake 1 and Uptake 2"). The affinity ($K_m$: affinity constant) and capacity ($V_m$: capacity constant) of the uptake 1 mechanism for MIBG is similar to those for norepinephrine ($K_m$ of $1.22 \pm 0.12$ μM for MIBG and $1.41 \pm 0.12$ μM for norepinephrine; $V_m$ of $64.3 \pm 3.3$ pmol/$10^6$ cells/10 min for MIBG and $36.6 \pm 7.2$ pmol/$10^6$ cells/10 min for norepinephrine). Uptake 1 predominates at low concentrations of both catecholamines and MIBG, whereas uptake 2 predominates at higher concentrations. It is therefore to be expected that MIBG administered in tracer amounts will primarily reflect uptake 1. Blocking experiments,

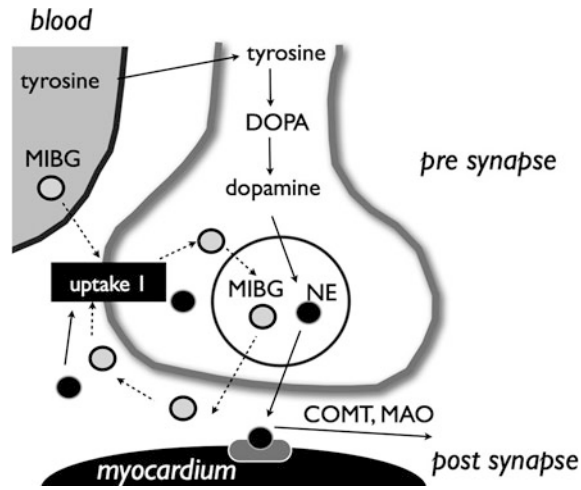


**Fig. 4.1** Sympathetic nerve terminal. Dihydroxyphenylalanine (*DOPA*); monoamine oxidase (*MAO*); catechol O-methyltransferase (*COMT*)

however, have shown that uptake 2 is responsible for up to 61% of cardiac MIBG uptake.

### 4.1.3 [$^{123}$I]-MIBG Myocardial Scintigraphy

In the past two decades, a large number of investigators have demonstrated decreased myocardial [$^{123}$I]-MIBG uptake in chronic HF patients and have shown that those with the lowest uptake tend to have the poorest prognosis [6–8]. There have also been findings suggesting that abnormalities of myocardial [$^{123}$I]-MIBG uptake may be predictive of increased risk for ventricular arrhythmia and sudden cardiac death (SCD) and implant cardiac defibrillator (ICD) discharge [9–11]. One factor that has constrained acceptance of cardiac [$^{123}$I]-MIBG imaging as a clinical management tool in HF has been the variability of technical aspects of the procedure. Although most publications include the heart-to-mediastinum (H/M) ratio as the measure of myocardial uptake, the methods used to obtain this parameter show considerable variation (Fig. 4.1).

#### 4.1.3.1 General Procedure for Planar [$^{123}$I]-MIBG Scintigraphy

In order to block thyroid uptake of free radioactive iodide, either 500 mg potassium perchlorate or 200 mg potassium iodide (10% solution) is orally administered. Thirty minutes later, ~185–370 MBq [$^{123}$I]-MIBG is administered intravenously. [$^{123}$I]-MIBG is internalized by presynaptic nerve endings of postganglionic neuronal cells through the energy-dependent uptake 1 system. A 15% energy window is usually used, centered on the 159 keV $^{123}$I photopeak. Anterior planar scintigraphic images are obtained 15 min (early) and 4 h (late) after injection and stored in a 128 × 128 matrix.

#### 4.1.3.2 Semiquantitative Parameters

The commonly used myocardial [$^{123}$I]-MIBG indices are the H/M ratio and myocardial washout. On anterior planar images, regions of interest (ROIs) are drawn over the heart and the mediastinum. The mean count density in each ROI is obtained, and the H/M ratio (specific activity/nonspecific activity) is calculated. Myocardial [$^{123}$I]-MIBG washout is calculated as the difference between the early and late H/M and expressed as a percentage of the early H/M:

$$\text{washout rate (WR)} = \left\{\frac{(\text{earlyH/M} - \text{lateH/M})}{\text{earlyH/M}}\right\} \times 100\,\%$$

The early H/M probably reflects the integrity of presynaptic nerve terminals and uptake 1 function. The late H/M combines information on neuronal function from uptake to release through the storage vesicle at the nerve terminals. Myocardial [$^{123}$I]-MIBG washout is an index of the degree of sympathetic drive. This implies that increased sympathetic activity is associated with high myocardial [$^{123}$I]-MIBG washout and low myocardial [$^{123}$I]-MIBG delayed uptake.

#### 4.1.3.3 Impact of ROI Definition

For [$^{123}$I]-MIBG, there are several ways to define the mediastinal (size and placement) and myocardial ROIs [i.e., myocardium, including the left ventricular (LV) cavity, versus myocardium excluding the LV cavity]. However, there are limited data on the impact of ROI definition on H/M ratios and myocardial washout. Somsen et al. [12] demonstrated in 25 healthy volunteers that [$^{123}$I]-MIBG semiquantitative parameters using an ROI of the myocardium including the LV showed the lowest interindividual and within-individual variability. In a large retrospective study, a uniform analysis with clear definition of the myocardial ROI (variable in size, including the LV cavity) and the mediastinal ROI (fixed size) showed remarkable consistency in interpretation between three blinded image evaluators. These findings suggest that rigorous and uniform analysis of cardiac [$^{123}$I]-MIBG semiquantitative parameters minimizes inter- and intra-individual variation.

#### 4.1.3.4 Influence of Collimation

The most well-validated influence on the measured late H/M is collimator type. In addition to the prime emission of 159-keV photons, $^{123}$I emits high-energy photons of >400 keV [~2.87%, main contributor 529 keV (1.28%)]. These high-energy photons lead to penetration of the collimator septa and cause scatter detected in the 159-KeV energy window. Septal penetration affects estimation of the H/M ratio in [$^{123}$I]-MIBG imaging with a low-energy (LE) collimator. Regardless, LE collimators are frequently used for imaging [$^{123}$I]-MIBG. Medium-energy (ME) collimators have been shown to improve quantitative accuracy in $^{123}$I studies. Therefore, to minimize the effects of septal penetration, the ME collimator is preferred. However, the use of ME collimation provides relatively low spatial resolution, which may hamper accurate estimation of activity in small regions through a partial volume effect. In brain single-photon-emission computed tomography (SPECT) imaging with [$^{123}$I]-labelled agents, collimation with low energy, high resolution (LEHR) is preferred, because high spatial resolution is required, head and brain tissue lead to a more or less homogeneous scatter, and the regions are mostly equidistant from the gamma camera. In cardiac scintigraphy with $^{123}$I labelled agents, however, H/M ratios are assessed from counts in relatively large regions, the thorax and abdomen lead to an inhomogeneous scatter, and the myocardium is not equidistant from the gamma camera, especially for SPECT imaging. In cardiac scintigraphy with [$^{123}$I]-labelled agents, the tradeoff between spatial resolution and septal penetration is therefore in favor of low septal penetration. Moreover, in a checker phantom, the use of ME collimation in cardiac scintigraphy with $^{123}$I showed contrast accuracy similar to technetium-99 m ($^{99m}$Tc).

Whereas these results would suggest that semiquantitative cardiac [$^{123}$I]-MIBG imaging might be best performed using ME collimators, there are practical limitations to such a recommendation. Almost all nuclear medicine procedures are now performed on a multihead gamma camera, and many dedicated dual-head cardiac cameras are not supplied with ME collimators. Despite these considerations, the use of ME collimation in cardiac scintigraphy with $^{123}$I is advocated.

### 4.1.4 Normal Databases of Cardiac MIBG

The quantitative approach played an important role in [$^{123}$I]-MIBG studies for estimating disease severity and prognosis, as discussed in other sections of this chapter. Most [$^{123}$I]-MIBG studies examining HF use the H/M ratio. It is unanimously reported that a low H/M ratio is a predictor of serious cardiac events, including cardiac death and lethal arrhythmia. The diagnostic thresholds of an H/M ratio of 1.2–1.7 are generally used for determining poor prognosis. Understanding normal [$^{123}$I]-MIBG databases is thus essential for properly applying MIBG studies in clinical practice. In this section, standardized [$^{123}$I]-MIBG parameters, normal values of the H/M ratio and WR, three-dimensional distribution of SPECT imaging, and the need for standardization are discussed [13].

#### 4.1.4.1 Definition of WR for Normal Databases

To calculate [$^{123}$I]-MIBG WR from the heart, most Japanese [$^{123}$I]-MIBG studies used the following formula:

$$\mathrm{WR} = \left(\left(\mathrm{H_{early}} - \mathrm{M_{early}}\right) - \left(\mathrm{H_{late}} - \mathrm{M_{late}}\right) \times \mathrm{k}\right) \Big/ \left(\mathrm{H_{early}} - \mathrm{M_{early}}\right),$$

where $H_{early}$ and $H_{late}$ are the average heart count in early and late imaging, and $M_{early}$ and $M_{late}$ are the average mediastinal count in early and late imaging. The coefficient k is the decay correction factor calculated as 1/(0.5^(t/13)), where t is time (h) between early and late imaging. The k value is 1.173 and 1.238 for 3 and 4 h, respectively.

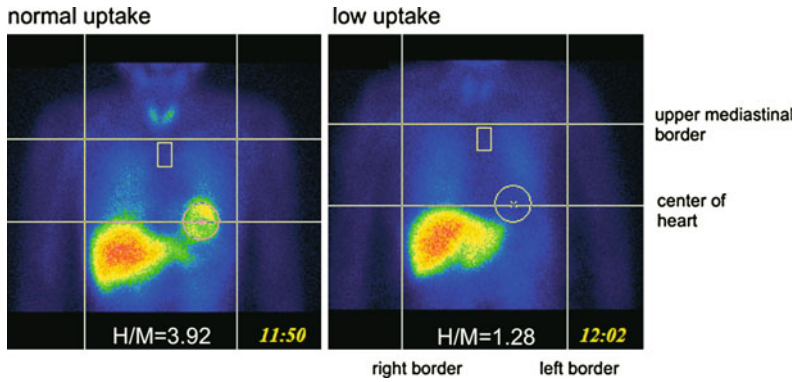


**Fig. 4.2** Semiautomatic region of interest (*ROI*) setting in individuals with normal and low [$^{123}$I] meta-iodobenzylguanidine (*MIBG*) uptake. *Horizontal* and *vertical lines* are automatic guides for defining chest region

#### 4.1.4.2 Semiautomatic Calculation of H/M Ratio (Smart MIBG Software)

Despite the recommendation for ROI location, ROI size and location are not fixed and can be a cause of variation among operators and institutions. A semiautomated method was developed for placing the mediastinal ROI after placing a circular ROI on the heart. The cardiac circular ROI is manually set in the center of the heart so as not to overlap lung activity, as some patients show very low uptake in the heart. Then, the following steps are utilized as an automatic algorithm:

- detection of the right border of the body
- detection of the midline of the mediastinum
- determination of the left border of the body
- determination of the upper border of the mediastinum
- setting the rectangular mediastinal ROI in the area of the lowest count; namely, 1/10 width of the body and 30% height of the mediastinum.

The algorithm of this semiautomatic algorithm is available in Japan using Smart [$^{123}$I]-MIBG Software (Fig. 4.2). The intraclass correlation coefficient from the semiautomated method showed excellent reproducibility for early ($r = 0.99$) and late ($r = 0.99$) imaging. The Bland–Altman plots demonstrated better agreement using the semiautomated method (95% limits from −0.11 to 0.10) compared with that in the manual method (−0.34 to 0.27).

#### 4.1.4.3 Normal Values of H/M Ratio and WR

It is well known that differences in data acquisition, particularly collimator type, affect H/M ratios, and these differences are obstacles for unifying multicenter data [13]. Standardization of [$^{123}$I]-MIBG cardiac sympathetic imaging proposed by the European Association of Nuclear Medicine (EANM) Cardiovascular Committee and the European Council of Nuclear Cardiology (ECNC) dealt with this issue.

**Table 4.1** Heart-to-mediastinum (H/M) ratio and washout rate (WR)

| Mean and normal ranges | | |
|---|---|---|
| H/M ratio[a] | | |
| | LE collimators | ME or LME collimators |
| Early | 2.39 ± 0.21 (1.97–2.81) | 2.76 ± 0.31 (2.14–3.38) |
| Late | 2.49 ± 0.25 (1.99–2.99) | 3.01 ± 0.35 (2.31–3.71) |
| Washout rate[b] | | |
| | Decay and BG correction: | 13% (3–22%) |
| | Decay correction without BG: | 16% (9–23%) |

*LE* low energy, *ME* medium energy, *LME* low-to-medium energy, *BG* background
[a] Mean and standard deviation
[b] Median and 10–90 percentile

Although LE high-resolution collimators are extensively available for common use, ME collimators are shown to provide superior semi-quantitative accuracy in [$^{123}$I]-MIBG studies [13]. Normal values of the H/M ratio were also significantly different when the Japanese Society of Nuclear Medicine (JSNM) Working Group MIBG databases were observed (Table 4.1). Although LE and ME types are two major groups, strictly speaking, LE general-purpose and LE HR collimators show slightly different characteristics for $^{123}$I for septal penetration from 529-KeV energy. Although the low-medium-energy (LME) collimator (Toshiba/Siemens, Japan) and ME collimator provide an identical H/M ratio, similar LME types from other venders may show different characteristics. Considering variations of collimator types among camera vendors, the JSNM proposed a calibration method based on specific phantoms designed for measuring H/M ratio. This type of calibration among institutions and camera types provides ME-collimator-comparable H/M values, even when using LE collimators, and results in distribution of normal H/M values from multiple institutions to a normal distribution. Deconvolution of a septal penetration method seems to be a promising method for correcting both two- and three-dimensional heart-to-calibration ratios.

Normal H/M ratio and WR values are shown in Table 4.1. Although WR is not largely influenced by collimator choice, factors of background correction, time-decay correction, and time between early and late imaging should be standardized. As WR reflects physiological dynamic changes, both background and decay corrections are recommended.

#### 4.1.4.4 Regional MIBG Distribution in SPECT Study

SPECT images are acquired by a single pass of 60 steps at 30 s per step (64 × 64 matrix), starting at a 45° right anterior oblique projection and proceeding counterclockwise to the 45° left posterior oblique projection. Data are reconstructed in short-, horizontal long-, and vertical long-axis tomograms, and scatter or attenuation correction may be applied.

When regional [$^{123}$I]-MIBG distribution is observed, factors of physical characteristics of $^{123}$I, pharmaceutical dynamics and relative count distribution in liver, heart, and lungs are related. [$^{123}$I]-MIBG distribution in the SPECT study is similar to that of perfusion imaging tracers, but the inferior accumulation is relatively lower in an [$^{123}$I]-MIBG study, in particular, for aged persons. The JSNM working group accumulated [$^{123}$I]-MIBG databases (both 360° and 180° rotations separately) from near-normal individuals who had no history of cardiac diseases and were not taking medications due to diabetes, hypertension, or dyslipidemia. The average and mean deviation of distribution patterns using a polar-map display is shown in Fig. 4.3. In late imaging, the inferior wall shows lower activity and a relatively large deviation, which is in agreement with our impression of clinical [$^{123}$I]-MIBG imaging. Heterogeneity of [$^{123}$I]-MIBG distribution is not artifacts but physiological phenomenon and correlate with sympathetic and vagal activities in normal individuals. To evaluate ischemic myocardial diseases, in which [$^{123}$I]-MIBG shows regional denervation in the ischemic or infarcted area, comparison between [$^{123}$I]-MIBG distribution in patients and optimal [$^{123}$I]-MIBG normal databases is essential. In the meantime, gated SPECT perfusion data should be interpreted in patients with ischemic cardiomyopathy to obtain information on a potential infarcted area and wall-motion kinetic. SPECT images can be scored using a point scale for visual evaluation of [$^{123}$I]-MIBG concentration in given cardiac segments, comparable with a myocardial perfusion imaging scoring approach. Careful interpretation should be performed, with knowledge of normal variants and potential artifacts.

#### 4.1.4.5 Applying [$^{123}$I]-MIBG to Multicenter Studies

To apply [$^{123}$I]-MIBG in multicenter studies, the following steps are required. First, the acquisition method for [$^{123}$I]-MIBG should be standardized, and guidelines as given by EANM

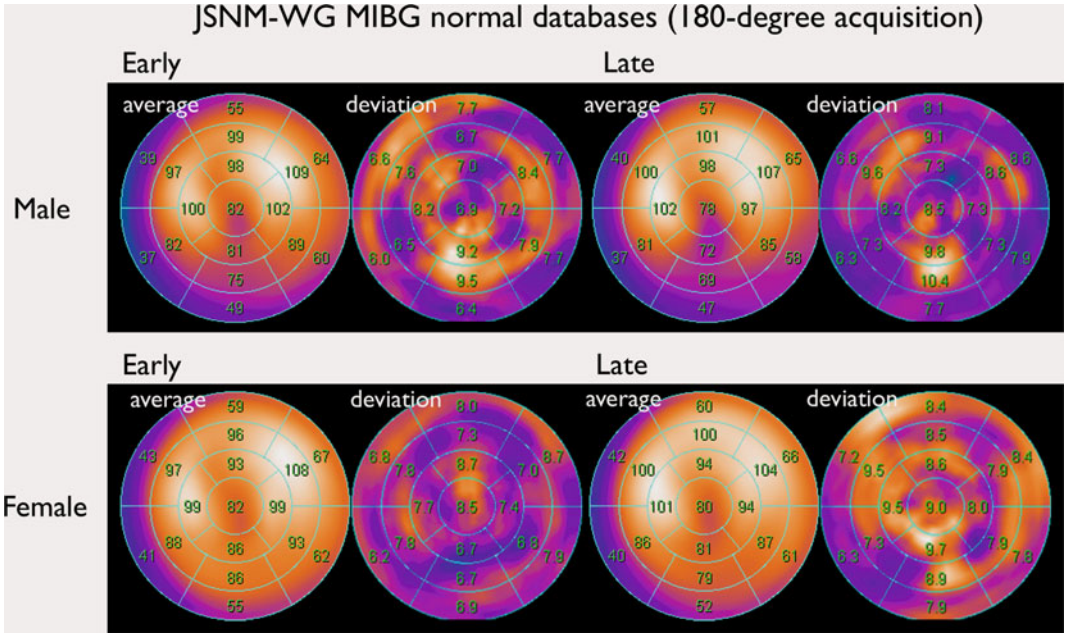


**Fig. 4.3** Standard databases from the Japanese society of nuclear medicine (*JSNM*) working group in male and female patients. Polar maps from 180° rotation acquisition, with averages and mean deviations

would be helpful [14]. Steps should include collimator types, matrix, acquisition time, camera rotation, and parameter calculation method. Second, the ROI setting for the H/M ratio should be standardized, and common software based on an automatic algorithm is important. Third, interinstitutional calibration is desirable, because various camera types from various venders each have their own characteristics for $^{123}$I imaging. Finally, normal databases and normal values should be provided to compare and follow-up patients over the long clinical course.

#### 4.1.4.6 Potential Pitfalls of Cardiac [$^{123}$I]-MIBG Imaging

Some potential technical pitfalls of [$^{123}$I]-MIBG scintigraphy can be identified. First, evaluation of SPECT images may be hampered by severely reduced myocardial uptake of the tracer in patients with severe HF (H/M ratio <1.2). Furthermore, the readers should be aware of the fact that [$^{123}$I]-MIBG shows reduced uptake in the inferior wall under normal conditions and particularly in elderly patients. Additionally, [$^{123}$I]-MIBG is taken by peripheral tissues supplied by sympathetic nerves, including tissue in liver, lungs, and thyroid gland [14]. In patients with excessive extracardiac (gastrointestinal or liver) [$^{123}$I]-MIBG uptake, evaluation of cardiac SPECT images may be difficult.

### 4.1.5 [$^{123}$I]-MIBG Imaging in Cardiac Pathologies

#### 4.1.5.1 In Ischemic Cardiomyopathy

Sympathetic nervous tissue is more sensitive to the effects of ischemia than is myocardial tissue. Uptake of [$^{123}$I]-MIBG is significantly reduced in areas of myocardial infarction (MI) and adjacent noninfarcted regions, as well as in areas with acute and chronic ischemia. It is likely that ischemia induces damage to sympathetic neurons, which may take a long time to regenerate, and that episodes of ischemia result in decreased [$^{123}$I]-MIBG uptake.

Matsunari et al. [15] report a dissociation between recovery of myocardial perfusion after an ischemic event and myocardial innervation,

as determined with [$^{123}$I]-MIBG SPECT. Despite considerable myocardial salvage following coronary artery reperfusion, [$^{123}$I]-MIBG images obtained a mean of 11 days after MI and reperfusion demonstrated a persistent area of myocardial denervation within the LV. This area was comparable with the area of ischemic myocardium at risk, as determined by myocardial perfusion SPECT during the acute ischemic event. Such modifications of cardiac neuronal function may have an important role in the pathophysiology of HF and arrhythmias, but further studies are warranted to determine the clinical value of innervation imaging in ischemic heart disease.

#### 4.1.5.2 In Arrhythmogenesis

Cardiovascular disease is the single most common cause of natural death in developed countries. SCD accounts for 50% of all cardiovascular deaths. The most common primary electrical event at the time of SCD is ventricular tachycardia (VT), which degenerates first to ventricular fibrillation (VF) and later to asystole.

SCD is usually attributed to structural heart disease, principally in the setting of acute or chronic MI. Ventricular tachyarrhythmias can be provoked in these patients with heterogeneous remodeling of sympathetic innervation, attributable to nerve growth and degeneration by physical or mental stress or by catecholamine application. On the other hand, adrenergic denervation of viable myocardium may also result in denervation supersensitivity, with exaggerated response of myocardium to sympathetic stimulation and increased vulnerability to ventricular arrhythmias. Therefore, when assessing the arrhythmogenic potential, variables such as presence of denervated but viable myocardium, severity of denervation, underlying level of sympathetic tone, and subsequent influences on local ventricular repolarization should be taken into account.

Whereas preventing arrhythmic deaths is generally ineffective with pharmacologic treatment, ICDs reduce the mortality rate in subgroups of patients thought to be at risk. However, identifying patients who most benefit from these devices remains difficult, and device implantation in patients who will not benefit leads to unnecessary morbidity, with increased medical costs. Arora et al. [9] evaluated the use of [$^{123}$I]-MIBG cardiac imaging (as means of local myocardial sympathetic innervation) and spectral analysis of heart-rate volume (HRV) (as means of central autonomic tone) in patients with ICDs. They studied 17 patients who had ICDs for various indications. The combined use of [$^{123}$I]-MIBG scintigraphy and HRV analysis correlated with the occurrence of an appropriate ICD discharge. Patients with ICD discharges had lower early H/M ratio, more extensive [$^{123}$I]-MIBG defects, and more [$^{123}$I]-MIBG/$^{99m}$Tc-sestamibi mismatch segments (denervation in areas of myocardial viability) compared with patients without previous ICD discharge. In addition, the ICD discharge group had reduced HRV values; suggesting abnormally increased sympathetic tone when compared with patients without previous ICD discharge. Therefore, the combined noninvasive evaluation of local cardiac autonomic innervation and systemic autonomic function by means of [$^{123}$I]-MIBG and HRV allowed identification of patients at risk for potentially fatal arrhythmias and SCD, who were most likely to benefit from an ICD.

In a phase 2, open-label, multicenter study that enrolled 50 patients with LV dysfunction and previous MI, Bax et al. [16] found that late [$^{123}$I]-MIBG SPECT defect score was the only variable that showed a significant difference between patients with and without positive electrophysiological studies. Further studies should demonstrate clinically relevant risk stratification of [$^{123}$I]-MIBG imaging, such as high negative predictive value (NPV) for life-threatening ventricular arrhythmias, especially in patients with ischemic heart disease and depressed LVEF. Boogers et al. [11] demonstrated in patients with severe (LVEF $< 35\%$) cardiomyopathy and ICD that late MIBG SPECT imaging was a better prognostic indicator of arrhythmias and cardiac death than perfusion and innervation mismatch SPECT imaging. One hundred and sixteen HF patients

referred for ICD therapy were enrolled. During a mean follow-up of 23 ± 15 months, appropriate ICD therapy (primary end point) was documented in 24 (21%) patients and appropriate ICD therapy or cardiac death (secondary end point) in 32 (28%) patients. Late [$^{123}$I]-MIBG SPECT defect score was an independent predictor for both end points. Patients with a large late [$^{123}$I]-MIBG SPECT defect (summed score >26) showed significantly more appropriate ICD therapy (52% versus 5%, $p < 0.01$) and appropriate ICD therapy or cardiac death (57% versus 10%, $p < 0.01$) than in patients with a small defect (summed score ≤26) at 3-year follow-up. Then, they concluded that cardiac sympathetic denervation predicts ventricular arrhythmias causing appropriate ICD therapy as well as the composite of appropriate ICD therapy or cardiac death.

#### 4.1.5.3 In Atrial Fibrillation

Akutsu et al. [17] investigated whether cardiac SNS activity measured by [$^{123}$I]-MIBG imaging would be associated with both the occurrence of HF and the transit to permanent atrial fibrillation in patients with paroxysmal atrial fibrillation. They evaluated 98 consecutive patients with idiopathic atrial fibrillation and preserved LVEF (>50%) during 4 ± 3.6 years. Lower late H/M ratio and lower LVEF were the independent predictors of transit to permanent atrial fibrillation, with adjusted hazard ratios of 3.44 [95% confidence interval (CI) 1.9–6.2, $p < 0.0001$] and 1.04 (95% CI 1.01–1.08, $p = 0.014$). They concluded that [$^{123}$I]-MIBG imaging may be a useful modality for predicting the development of atrial fibrillation.

#### 4.1.5.4 Risk Stratification of Patients with Heart Failure

Long-term prognosis of patients with HF remains poor, with a 5-year mortality rate of 59% for men and 45% for women. Furthermore, prognosis in HF can be determined reliably only in populations and not in individuals. To improve survival, adequate risk stratification is needed. The most significant predictors of survival in clinical management include decreasing LVEF, worsening New York Heart Association (NYHA) functional status, degree of hyponatremia, decreasing peak exercise oxygen uptake ($V0_2$), decreasing hematocrit, resting tachycardia, renal insufficiency, intolerance to conventional therapy, and refractory volume overload. Impaired cardiac adrenergic innervation as assessed by [$^{123}$I]-MIBG imaging is strongly related to mortality in patients with HF, independently of its cause. Merlet et al. [6] studied the prognostic value of [$^{123}$I]-MIBG scintigraphy compared with that of other noninvasive cardiac imaging indices in 90 patients with either ischemic ($n = 24$) or idiopathic ($n = 66$) cardiomyopathy. During a follow-up period of 1–27 months, ten patients underwent cardiac transplantation, and 22 died. Among all clinical and imaging variables (cardiac [$^{123}$I]-MIBG uptake, radionuclide LVEF, X-ray cardiothoracic ratio, and echographic end-diastolic diameter), the late H/M ratio was the best predictor of event-free survival. The same authors [7] subsequently evaluated 112 patients with HF and dilated cardiomyopathy (DCM) (NYHA classes II–IV, LVEF < 40%, LV end-diastolic diameter 70 ± 8 mm, and pulmonary capillary wedge pressure 19 ± 8 mmHg). Among all variables (cardiac [$^{123}$I]-MIBG uptake, circulating NE concentration, LVEF, peak $V0_2$, X-ray cardiothoracic ratio, M-mode echographic end-diastolic diameter, and right-sided heart catheterization parameters), only late H/M ratio and LVEF were independent predictors for mortality (mean follow-up 27 ± 20 months). In addition, [$^{123}$I]-MIBG uptake and circulating NE concentration were the only independent predictors for life duration. In both studies by those authors, a late H/M ratio of 1.2 was used to identify reduced [$^{123}$I]-MIBG uptake. The low value of H/M ratio (1.2) was due to the absence or nonrecommendation of certain treatment in HF, such as beta-blockers, angiotensin receptor blockers, and aldosterone antagonists within the (1988–1990) period.

Cohen-Solal et al. [18] showed in a study of 93 HF patients and LV dysfunction that late H/M ratio was reduced and correlated with other predictors of prognosis, such as LVEF, cardiac index, pulmonary wedge pressure, and peak $V0_2$. Moreover, a late H/M ratio $\leq$1.2 and peak $V0_2$ were predictive of death or cardiac transplantation over 10 $\pm$ 8 months of follow-up, whereas early H/M ratio and WR were not. Wakabayashi et al. studied 414 patients (42% with symptomatic HF) with [$^{123}$I]-MIBG scintigraphy. Over a mean follow-up of 22 $\pm$ 7 months, 37 cardiac deaths occurred. Late H/M ratio was the most powerful predictor of cardiac mortality among the variables. A late H/M ratio $\leq$1.74, age >60 years, history of MI, and NYHA class III or IV strongly indicated poor clinical outcomes. Wakabayashi et al. [19] reported [$^{123}$I]-MIBG imaging as the most powerful independent long-term prognostic value for both ischemic ($n = 76$) and idiopathic ($n = 56$) cardiomyopathy patients, which hints at cardiac autonomic dysfunction as a common end point leading to cardiac death, regardless of the underlying etiology of the cardiac disease. Late H/M ratio was the most powerful independent predictor of cardiac mortality in both groups of patients (superior to early H/M ratio and WR) and had an identical threshold (1.82) for both groups for identifying patients at risk of cardiac death. Nevertheless, when analyzing patients with LVEF <40%, the upper cutoff value of late H/M ratio was 1.50 for ischemic patients and 2.02 for idiopathic patients, which may suggest that the underlying etiology of HF relates to the threshold of the late H/M ratio for differentiation of high-risk patients. This study was designed, however, before optimal up-to-date HF treatment, and derived results may not translate to current cohorts of HF patients.

All these results suggest that the late H/M ratio may be the best prognostic parameter that can be obtained from planar [$^{123}$I]-MIBG imaging. Agostini et al. [20] showed in a European retrospective study the strong prognostic value of late H/M ratio in patients with HF. Blind review and prospective quantitative reanalysis of the late H/M ratio of 290 patients with ischemic and nonischemic HF (NYHA class II–IV, 262 patients with LVEF <50%) with follow-up data for 2 years permitted the identification of potential late H/M ratio threshold values for defining groups with high and very low likelihood of major cardiac events. Mean H/M ratio was significantly different between patients with and without events (1.51 versus 1.97). Based on receiver operating characteristic (ROC) curve analysis, a threshold value for H/M ratio of 1.75 yielded a sensitivity of 84% and specificity of 60% to predict events. Based on this threshold value, the 2-year event-free survival was 62% for late H/M ratio <1.75 versus 95% for late H/M ratio of 1.75. Logistic regression showed late H/M ratio and LVEF as the only significant predictors of major cardiac events. When the late H/M ratios were divided into quartiles, the 2-year event-free survival rates in the lowest (1.45) and highest (2.17) quartiles were 52 and 98%, respectively. Tamaki et al. [21] prospectively compared the predictive value of cardiac [$^{123}$I]-MIBG imaging for SCD with that of the signal-averaged electrocardiogram (SA-ECG), HRV, and QT dispersion in 106 consecutive outpatients with mild-to-moderate stable HF due to ischemic heart disease in 55 patients and idiopathic DCM in 51 patients. During a follow-up period of 65 $\pm$ 31 months, 18 of 106 patients died suddenly. A multivariate Cox analysis revealed that only WR and LVEF were significantly and independently associated with SCD. Patients with an abnormal WR (>27%) had a significantly higher risk of SCD (adjusted HR: 4.79, 95% CI 1.55–14.76). Even when confined to patients with LVEF >35%, SCD was significantly more frequently observed in patients with than without abnormal WR.

In a systematic review, Verberne et al. [8] assessed existing evidence on the prognostic value of semiquantitative parameters of myocardial [$^{123}$I]-MIBG uptake in patients with HF. The pooled HR estimates for cardiac death and cardiac events associated with [$^{123}$I]-MIBG washout were 1.72 (95% CI 1.72–2.52; $p = 0.006$) and 1.08 (95% CI 1.03–1.12; $p < 0.001$), respectively. Pooled HR estimates for cardiac death and cardiac events associated

with early H/M and late H/M ratios showed significant heterogeneity ($I^2 \geq 75\%$). Limiting pooling to the qualitative best three studies rendered $I^2$ insignificant ($I^2 = 0$) and resulted in a pooled HR of late H/M ratio for cardiac death of 1.82 (95% CI 0.80–4.12; $p = 0.15$) and for cardiac events of 1.98 (95% CI 1.57–2.50; $p < 0.001$). These results indicate that patients with CHF and decreased late H/M ratio or increased myocardial [$^{123}$I]-MIBG WR have a worse prognosis than those with normal semi-quantitative myocardial [$^{123}$I]-MIBG parameters. Jacobson et al. [10], in the largest prospective multicenter trial, showed the potential role of cardiac [$^{123}$I]-MIBG imaging in HF is the AdreView Myocardial Imaging for Risk Evaluation in Heart Failure (ADMIRE-HF) trial in which [$^{123}$I]-MIBG myocardial imaging was performed in 961 patients with HF (NYHA II/III) and a reduced LVEF (<35%). A predefined late H/M ratio cutoff value of 1.6 was used. During a 2-year follow-up, 25% of patients had a cardiac event (i.e., NYHA functional class progression, potentially life-threatening arrhythmic event, or cardiac death). Cox proportional hazard analysis showed that there was a highly significant relationship between time to HF-related events and the H/M ratio, independent of other commonly measured parameters such as LVEF and brain natriuretic peptide (BNP). In addition, the study showed a clear association between severity of myocardial sympathetic neuronal dysfunction and risk for subsequent cardiac death. Gerson et al. [22] demonstrated the prognostic power of [$^{123}$I]-MIBG for detecting the clinically relevant end point of HF progression in the subgroup of patients with diabetes in the ADMIRE-HF trial. H/M ratio can complement data derived from LVEF, B-type natriuretic peptide, and diabetes status for predicting HF progression.

The Seattle Heart Failure Model (SHFM) is a multivariate model that predicts survival in patients with HF. Kuramoto et al. [23] showed that cardiac MIBG WR imaging improved the prognostic power of the SHFM in 106 patients with chronic HF (LVEF < 40%) during a mean follow-up of 6.8 ± 3.5 years. In the same field, Ketchum et al. [24] investigated combining [$^{123}$I]-MIBG cardiac imaging and the SHFM to predict mortality in the ADMIRE-HF EXtension (ADMIRE-HFX) trial. Survival data from the 961 NYHA II–III participants in the original study and additional follow-up on 470 participants was included in that analysis. Mortality predictions from the SHFM, the late H/M ratio, and a combined model were compared. There were 101 deaths during a median follow-up of 2 years. Cox modeling showed improvement in SHFM discriminant ability for all-cause mortality with the addition of H/M ratio ($p < 0.0001$). For a 1-standard deviation (SD) increase in SHFM score, risk increased by 82% ($p < 0.001$), whereas for a 1-SD decrease in H/M ratio, the risk increased 60% ($p < 0.001$). Observed 2-year survival in the highest risk SHFM participants varied from 54% with H/M ratio <1.2 to 100% with H/M ratio ≥1.80. The integrated discrimination improvement was significant ($p < 0.0001$), whereas the area under the receiver-operator characteristic curve (AUC) at 1 year improved from 0.658 for H/M ratio and from 0.692 for SHFM to 0.731 for the combined model ($p = 0.03$). The authors concluded that abnormalities of H/M ratio and SHFM risk scores are associated with increased mortality rates in HF patients. A combined model offers additional prognostic information over either score alone.

Verberne et al. [25] determined the most appropriate prognostic endpoint for use of MIBG imaging based upon aggregate results from multiple studies published in the past decade. Then, published studies from Europe and the United States were identified for which original individual patient data for H/M ratio from late (3–5 h) planar MIBG imaging were available. Data submitted by the participating investigators were pooled, and Cox proportional hazards analyses were performed. Endpoints of all-cause mortality, cardiac mortality, arrhythmic events, and heart transplantation were investigated to determine which one provided the strongest prognostic significance for MIBG imaging data. Data from six studies with a total of 636 HF patients were retrieved. The majority

of patients was male (78%), had a decreased LVEF (31.1 ± 12.5%), and a mean late H/M ratio of 1.67 ± 0.47 (first quintile ≤ 1.32; second to fourth quintile 1.33–1.97, fifth quintile ≥ 1.98). During follow-up (mean 42.1 ± 26.5 months), there were 95 deaths, 79 cardiac deaths, 38 arrhythmic events, and 57 heart transplants. In univariate Cox analyses, late H/M ratio was a significant predictor of all event categories, but the highest Chi squares and lowest HRs were for all-cause ($\chi^2 = 17.68$, HR = 0.37, 95% CI 0.22–0.61) and cardiac ($\chi^2 = 14.57$, HR = 0.37, 95% CI 0.21–0.65) mortality. In multivariate analysis for the composite of any event, H/M ratio was a significant predictor (HR = 0.53, 95% CI 0.36–0.78), with LVEF, gender, and NYHA class also included in the model. In similar analyses for the individual event categories in patients with reduced LVEF (<50%, $n = 580$), H/M ratio was a significant predictor of all-cause (HR = 0.49, 95% CI 0.27–0.89) and cardiac (HR = 0.45, 95% CI 0.23–0.87) mortality, with LVEF, age, and HF etiology also included in the model. The same four variables were significant in models using a dichotomous H/M ratio split at 1.20 (1 SD below the mean), with patients with late H/M ratio <1.2 having the highest mortality (median survival 71 months) and with an H/M HR for cardiac death and all-cause mortality of 0.39 (95% CI 0.22–0.71) and 0.49 (95% CI 0.28–0.86), respectively. Finally, late H/M ratio is strongest as a univariate predictor of all-cause and cardiac mortality in HF patients. In multivariate analyses, MIBG imaging tends to be strongest as a predictor of cardiac death.

#### 4.1.5.5 In Treatment Assessment of HF Patients

Neurohormonal blockers [beta-blockers, angiotensin-converting enzyme inhibitors (ACEIs), angiotensin receptor blockers (ARBs), and aldosterone antagonists) are the main treatments for HF. However, the appropriate time to initiate treatment and the best sequence and combination of medications are uncertain at present. Cardiac [$^{123}$I]-MIBG imaging can detect drug-induced changes in cardiac adrenergic activity. Gerson et al. [26] studied the effect of chronic carvedilol treatment in patients with HF and cardiac sympathetic nerve dysfunction of varying severity due to idiopathic cardiomyopathy. Most patients showed a favorable response in LV function to the treatment, regardless of the baseline level of cardiac SNS function, as assessed by cardiac [$^{123}$I]-MIBG imaging. Patients with relatively advanced cardiac sympathetic dysfunction (baseline late H/M ratio <1.40 in [$^{123}$I]-MIBG studies) were the most likely to show evidence of improved cardiac SNS function in response to carvedilol treatment. Kasama et al. [27], taking into account that [$^{123}$I]-MIBG imaging improves medical treatment for HF, analyzed the usefulness of serial [$^{123}$I]-MIBG studies for prognostication in 208 patients with stabilized mild to moderate HF and LVEF <45% of both ischemic and nonischemic origin. The [$^{123}$I]-MIBG and ECG studies were performed once patients were stabilized and after 6 months of treatment that included ACEIs, ARBs, $\beta$-blockers, loop diuretics, and spironolactone. Treatment did not change during the follow-up. Fifty-six patients experienced fatal cardiac events during the study period (13 SCD). Clinical characteristics were similar in both noncardiac and cardiac death groups. With respect to pharmacotherapy in the two groups, only the use of $\beta$-blockers in the noncardiac death group was significantly higher than in the cardiac death group. Variation in the WR between the sequential [$^{123}$I]-MIBG (Δ-WR) was the only independent predictor of cardiac death. The Δ-WR was significantly lower in the noncardiac death group (<−5%) than that in the cardiac death group (≥−5%). Moreover, this parameter was also useful for predicting SCD in patients with HF, indicating that serial [$^{123}$I]-MIBG imaging is useful for predicting cardiac death and SCD in stabilized patients with HF.

In Caen Hospital, we followed severe heart failure patients under treatment with LVAD(Jarvik 2000 and Heartmate II) (unpublished data). Symptom assessment based on NYHA class, BNP level, peak $V0_2$, and number

of episodes of ventricular arrhythmias recorded by implantable defibrillators were searched for every patient. MIBG scintigraphy , BNP, and peak $V0_2$ were measured during the same week. Five patients had severe HF, were in NYHA stage 4 before implantation of the LVAD, with low ejection fraction (LVEF $< 0.3$) and high BNP levels (>1,000 pg/mL). Peak $VO_2$ measured in four patients was <12 mL/kg per min. Symptom assessment, BNP level, and peak $VO_2$ improved significantly under LVAD support (for all patients: NYHA = 2, BNP level < 400 pg/mL, peak $VO_2 > 15$ mL/kg per min). However, H/M ratio remained very low in all patients, suggesting the absence of improvement of sympathetic neuronal function (H/M ratio = 1.46 ± 0.2; range 1.2–1.7; normal range: 2.2 ± 0.3), even after long-term support (up to 68 months). Interestingly, no patient presented symptomatic or asymptomatic ventricular arrhythmias during follow-up. Whereas classical markers of chronic HF severity improved significantly under LVAD and were considered to be of good prognosis, H/M ratio remained very low, suggesting the absence of improvement in sympathetic neuronal integrity under LVAD.

#### 4.1.5.6 In Stress Cardiomyopathy

Takotsubo syndrome is a clinical entity characterized by acute but rapidly reversible LV systolic dysfunction, with midventricular-wall-motion abnormalities, apical akinesia or dyskinesia, and preserved or hyperkinetic contractile function of the basal LV segments in the absence of atherosclerotic coronary artery disease (CAD) triggered by acute emotional or physical stress. Several hypotheses are advocated as possible pathophysiologic mechanisms, including catecholamine-mediated multivessel epicardial spasm, microvascular coronary spasm, and direct catecholamine-mediated myocyte toxicity. However, it remains unclear whether these abnormalities are the primary cause of the disorder or secondary events. As the entity is much more common in postmenopausal women, important influences of sex hormones on the sympathetic neurohormonal axis and on coronary vasoreactivity have been suggested. [$^{123}$I]-MIBG imaging shows reduced uptake in the akinetic LV apex, with normal or only mildly reduced perfusion within this region [28].

## 4.2 Cardiac Neurotransmission Imaging Using [$^{123}$I]-MIBG Scintigraphy in Brain Disease

Application of [$^{123}$I]-MIBG in neurological diseases has increased due to the increasing number of [$^{123}$I]-MIBG images in a group of Lewy body diseases (LBD). MIBG study demonstrated its effectiveness in differentiating LBD from other types of neurodegenerative diseases with cognitive impairment. Clinical application of [$^{123}$I]-MIBG began with the observation of markedly reduced cardiac [$^{123}$I]-MIBG uptake in patients with neurological diseases presenting orthostatic hypotension and other autonomic failures [29]. Thereafter, decreased cardiac [$^{123}$I]-MIBG activity in patients with Parkinson's disease and dementia with Lewy bodies has been extensively investigated in comparison with other types of neurological disorders [30]. These disease entities showed a common pathological base of Lewy-body deposition in multiple organs. Subsequently, low [$^{123}$I]-MIBG uptake has also been reported in patients with pure autonomic failure and rapid-eye-movement sleep-behavior disorder. In the neurological patient groups, reduced [$^{123}$I]-MIBG activity in the heart has been recognized as a biomarker of LBD.

### 4.2.1 Pathological Backgrounds

The reason for decreased [$^{123}$I]-MIBG uptake is supported by pathological investigations. The important issue was why brain disorder decreased [$^{123}$I]-MIBG uptake in the heart. The decrease in myocardial [$^{123}$I]-MIBG uptake reflected the fact that abnormality is not only restricted to the brain

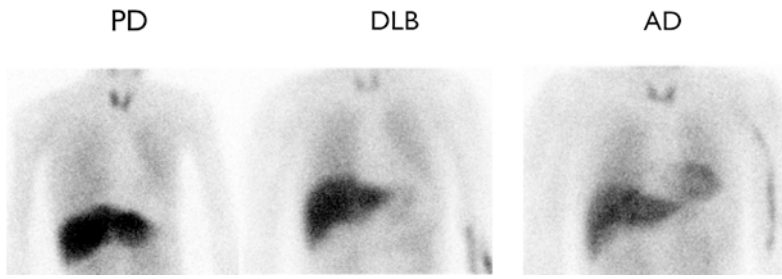


**Fig. 4.4** [$^{123}$I]-MIBG imaging in patients with Parkinson's disease (*PD*, *left*), dementia with Lewy bodies (*DLB*, *middle*), and Alzheimer's disease (*AD*, *right*). Anterior planar images

but involves more extensive derangement of sympathetic neuronal function in multiple organs. A major lesion in Parkinson's disease is neuronal degeneration with an appearance of Lewy bodies, and loss of neurons in the following predilection sites was demonstrated by post-mortem studies [31]. Lewy bodies distributed widely in the hypothalamus and sympathetic and parasympathetic systems were also found in the enteric nervous system of the alimentary tracts, cardiac plexus, pelvic plexus, and adrenal medulla. Lewy bodies and α-synuclein-positive neurites were identified in hearts of patients with Parkinson's disease [32]. In an autopsy-proven patient with Parkinson's disease, cardiac plexus was more heavily involved than were sympathetic ganglia, which could have been direct evidence for explaining low cardiac MIBG uptake. The only neuropathological requirement for diagnosing dementia with Lewy bodies was the presence of Lewy bodies somewhere in the brain of a patient with a clinical history of dementia [33]. Central, core, and suggestive features have been summarized from clinical viewpoints in the consortium on dementia with Lewy bodies. However, diagnosis of LBD seems to be underestimated. Its differential diagnosis from Alzheimer's disease, which is the most common type of dementia, and other pathology of dementia-related diseases is still challenging, even for neurologists. As Parkinson's disease and dementia with Lewy bodies are considered as a generalized neuronal disorder, myocardial [$^{123}$I]-MIBG defects could be representative of pathological progression of extensive autonomic involvement.

### 4.2.2 [$^{123}$I]-MIBG Findings in Parkinson's Disease

Typical [$^{123}$I]-MIBG images of patients with Parkinson's disease, dementia with Lewy bodies, and Alzheimer's disease are shown in Fig. 4.4. In patients with Parkinson's disease, decrease in cardiac [$^{123}$I]-MIBG uptake is observed in 80–90%. [$^{123}$I]-MIBG uptake is globally decreased in both planar imaging and SPECT studies. The decrease is observed even in early-onset stages. However, as some patients show normal myocardial activity in the mild or early stage, normal [$^{123}$I]-MIBG uptake cannot readily exclude the possibility of Parkinson's disease. Although [$^{123}$I]-MIBG activity seems to decrease progressively during the clinical course, the temporal change from a normal uptake to the typically decreased [$^{123}$I]-MIBG uptake was not well demonstrated in the same cohort. In studies with a large number of patients, however, stage progression and H/M ratio showed weak negative correlation. Although WR was also calculated to be higher in patients with Parkinson's disease, it should be carefully interpreted, as initial uptake is low and washout variation becomes large. Those who have orthostatic hypotension tend to show a low [$^{123}$I]-MIBG uptake. Based on a meta-analysis of studies with a total of 246 cases of Parkinson's disease and 45 of multiple system atrophy, overall sensitivity to positively identify patients with Parkinson's disease was 89.7% and specificity was 94.6%. When H/M ratios were surveyed in the literature, early H/M ratios ranged from 1.3 to 1.7 (median 1.58) and late H/M

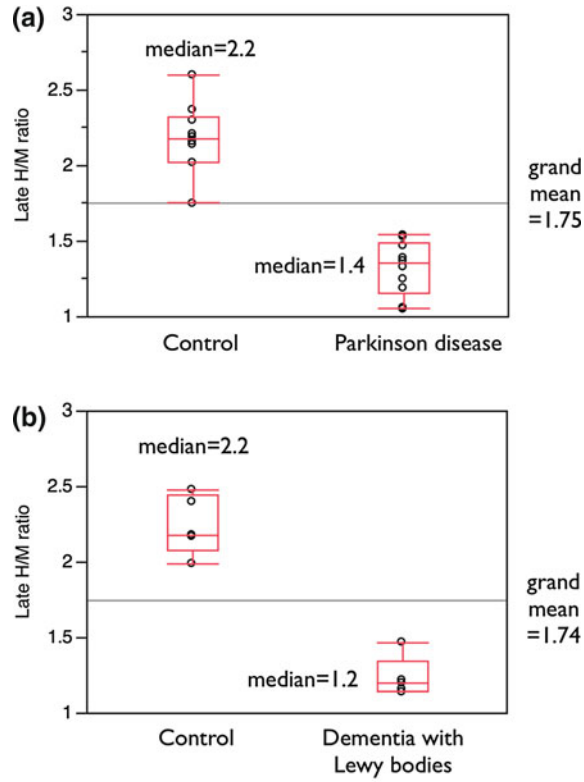


**Fig. 4.5** **a** Distribution of average late heart-to-mediastinum (*H/M*) ratios in ten studies of patients with Parkinson's disease and controls [Iwasa et al. (Acta Neurol Scand 1998;97:303), Yoshita et al. (J Neurol Sci 1998;155:60), Orimo et al. (J Neurol Neurosurg Psychiatry 1999;67:189), Braune et al. (Acta Neurol Scand 1998;97:307), Reinhardt et al. (Eur J Nucl Med 2000;27:595), Druschky et al. (J Neurol Sci 2000;175:3), Takatsu et al. (J Nucl Med 2000;41:71), Taki et al. (Eur J Nucl Med 2000;27:566), Hamada et al. (J Neurol Neurosurg Psychiatry 2003;74:423), and Orimo et al. (Intern Med 2003;42:127)]. **b** Distribution of average late H/M ratios in five studies of patients with dementia with Lewy bodies and controls [Watanabe et al. (J Neurol Neurosurg Psychiatry 2001;70:781), Saiki et al. (J Neurol Sci 2004;220:105), Yoshita et al. (Neurology 2006;66:1850), Kashihara et al. (J Nucl Med 2006;47:1099), and Novellino et al. (Neurobiology of Aging 2010;31:1903)]

ratios from 1.1 to 1.6 (median 1.25), showing significantly lower values than in control patients [30]. The distribution of average H/M ratio values in ten studies of both Parkinson disease and control patients is shown in Fig. 4.5a.

### 4.2.3 [$^{123}$I]-MIBG Findings in Dementia with Lewy Bodies

A meta-analysis of [$^{123}$I]-MIBG in dementia with Lewy bodies showed that pooled sensitivity of [$^{123}$I]-MIBG scintigraphy for differentiating from other dementia was 98% (95% CI 94–100) and specificity was 94% (95% CI 90–97) [34]. A 4-year follow-up of 65 patients showed H/M ratio significantly decreased in patients with dementia with Lewy bodies compared with that of the other neurodegenerative diseases, and the best H/M ratio cutoff point was 1.36, with sensitivity 94% and specificity 96% [35]. Regarding differential diagnosis between dementia with Lewy bodies and Alzheimer's disease, a Japanese study showed that late H/M ratio had sensitivity of 100%, specificity of 100%, and

positive predictive value (PPV) of 100% at a cutoff value of 1.68 [36]. The distribution of average H/M values in five studies in which H/M ratios of both patients with dementia with Lewy bodies and control patients were available, is shown in Fig. 4.5b. In the consortium guidelines, abnormally low [$^{123}$I]-MIBG uptake in myocardial scintigraphy is suggested as being one of the supportive features. A multicenter study for determining the role of [$^{123}$I]-MIBG study in patients with dementia with Lewy bodies is under investigation in Japan [37]. Preliminary data indicate that late H/M ratio was $2.55 \pm 0.53$ for Alzheimer's disease and $1.54 \pm 0.60$ for dementia with Lewy bodies ($p < 0.0001$) after standardization of the H/M ratio among institutions.

King et al. show in the meta-analysis of [$^{123}$I]-MIBG cardiac scintigraphy for diagnosing Lewy-body-related disorders that the AUC was 0.987 at the cluster discriminatory late H/M threshold of 1.77. They concluded that [$^{123}$I]-MIBG scintigraphy can accurately distinguish between two movement disorders (Parkinson's disease and multiple-system atrophy) and between two common causes of dementia (Alzheimer's disease and dementia with Lewy bodies) [38].

Some studies indicated positive differences in perfusion patterns on brain perfusion SPECT and [$^{18}$F]-fluorodeoxyglucose positron-emission tomography ([$^{18}$F]FDG-PET). A greater degree of occipital hypoperfusion or hypometabolism was observed in patients with dementia with Lewy bodies in comparison to patients with Alzheimer's disease. However, when the [$^{123}$I]-MIBG study was compared with brain perfusion SPECT, it seemed to be more accurate as a means of discriminating these two diseases [39].

### 4.2.4 Other Neurological Diseases

Marked reduction in [$^{123}$I]-MIBG uptake is observed in Parkinson's disease, dementia with Lewy bodies, and pure autonomic failure, which are recognized as characteristic findings of LBD. Markedly reduced cardiac [$^{123}$I]-MIBG uptake is also found in idiopathic rapid-eye-movement sleep-behavior disorder. This finding is consistent with the loss of sympathetic terminals and suggests a *form fruste* (i.e., an incomplete form) of LBD. More experience using [$^{123}$I]-MIBG studies is required for this group of patients. As it is well known that various types of cardiac diseases exhibit low [$^{123}$I]-MIBG uptake, patients with underlying diseases should be comprehensively assessed.

**Table 4.2** Indications for [$^{123}$I]-MIBG imaging

| Pathology | |
|---|---|
| Cardiac | Neurological |
| Ischemic injury or denervation | Lewy body diseases |
| Area at risk in acute coronary syndrome | Parkinson's disease |
| Denervated but viable myocardium | Dementia with Lewy bodies |
| Infarction | Pure autonomic failure |
| Cardiomyopathy | |
| Heart failure | |
| Therapeutic effect | |
| Prognosis | |
| Arrhythmia | |
| Life-threatening arrhythmia and cardiac death | |

## 4.3 Conclusions

Evidence provided by [$^{123}$I]-MIBG scintigraphy implicates the SNS in the development and progression of HF (Table 4.2). Sympathetic myocardial innervation as assessed with [$^{123}$I]-MIBG has a powerful prognostic value in HF patients. CHF patients with the lowest myocardial [$^{123}$I]-MIBG uptake tend to have the poorest prognosis. However, additional studies are necessary to determine whether [$^{123}$I]-MIBG can assist in triaging patients being considered for ICD placement.

In the meantime, in neurology, cardiac presynaptic reuptake and storage of sympathetic neurotransmitters can be measured and analyzed

in vivo using myocardial [$^{123}$I]-MIBG scintigraphy in patient with parkinsonism. Assessing cardiac neuronal function can be helpful in characterizing Parkinson's disease and multiple system atrophy and between two common causes of dementia: Alzheimer's disease and dementia with Lewy bodies (Table 4.2).

Advances in cardiac neurotransmission SPECT imaging include the development of tracers for adrenergic receptors, which may allow differentiation of structural denervation (loss of nerve terminals) from dysinnervation (down-regulation of the uptake l mechanism). Future challenges include development of tracers for parasympathetic neurotransmission and other receptor systems, as well as targeting second-messenger molecules.

## References


1. Carrio I (2001) Cardiac neurotransmission imaging. J Nucl Med 42:1062–1076
2. Zipes DP (1995) Autonomic modulation of cardiac arrhythmias. In: Zipes DP, Jalife J (eds) Cardiac electrophysiology: from cell to bedside, 2nd edn. Saunders Company, Phildelphia, pp 441–442
3. Bristow MR (1984) The adrenergic nervous system in heart failure. N Engl J Med 311:850–851
4. Wieland DM, Wu J, Brown LE, Mangner TJ, Swanson DP, Beierwaltes WH (1980) Radiolabeled adrenergi neuron-blocking agents: adrenomedullary imaging with [$^{131}$I] iodobenzylguanidine. J Nucl Med 21:349–353
5. Kline RC, Swanson DP, Wieland DM, Thrall JH, Gross MD, Pitt B, Beierwaltes WH (1981) Myocardial imaging in man with I-$^{123}$ meta-iodobenzylguanidine. J Nucl Med 22:129–132
6. Merlet P, Valette H, Dubois-Rande et al (1992) Prognostic value of cardiac metaiodobenzylguanidine imaging in patients with heart failure. J Nucl Med 33:471–477
7. Merlet P, Benvenuti C, Moyse D et al (1999) Prognostic value of MIBG imaging in idiopathic dilated cardiomyopathy. J Nucl Med 40:917–923
8. Verberne HJ, Brewster LM, Somsen GA, van Eck-Smit BLF (2008) Prognostic value of myocardial $^{123}$I-metaiodobenzylguanidine (MIBG) parameters in patients with heart failure: a systematic review. Eur Heart J 29:1147–1159
9. Arora R, Ferrick KJ, Nakata T et al (2003) I-$^{123}$ MIBG imaging and heart rate variability analysis to predict the need for an implantable cardioverter defibrillator. J Nucl Cardiol 10:121–131
10. Jacobson AF, Senior R, Cerqueira MD et al (2010) Myocardial iodine-123 meta-iodobenzylguanidine imaging and cardiac events in heart failure results of the prospective ADMIRE-HF (adreview myocardial imaging for risk evaluation in heart failure) study. J Am Coll Cardiol 55:2212–2221
11. Boogers MJ, Borleffs CJ, Henneman MM et al (2010) Cardiac sympathetic denervation assessed with 123-iodine metaiodobenzylguanidine imaging predicts ventricular arrhythmias in implantable cardioverter-defibrillator patients. J Am Coll Cardiol 55:2769–2777
12. Somsen GA, Borm JJ, Dubois EA, Schook MB, van der Wall EE, van Royen EA (1996) Cardiac $^{123}$I-MIBG uptake is affected by variable uptake in reference regions: implications for interpretation in clinical studies. Nucl Med Commun 17:872–876
13. Nakajima K (2010) Normal values for nuclear cardiology: Japanese databases for myocardial perfusion, fatty acid and sympathetic imaging and left ventricular function. Ann Nucl Med 24:125–135
14. Flotats A, Carrio I, Agostini D et al (2010) Proposal for standardization of $^{123}$I-metaiodobenzylguanidine (MIBG) cardiac sympathetic imaging by the EANM cardiovascular committee and the European council of nuclear cardiology. Eur J Nucl Med Mol Imaging 37:1802–1812
15. Matsunari I, Schricke U, Bengel FM et al (2000) Extent of cardiac sympathetic neuronal damage is determined by the area of ischemia in patients with acute coronary syndrome. Circulation 101:2579–2585
16. Bax JJ, Kraft 0, Buxton AE et al (2008) [$^{123}$I]-MIBG Scintigraphy to predict inducibility of ventricular arrhythmias on cardiac electrophysiology testing: a prospective multicenter pilot study. Circ Cardiovasc Imaging 1:131–140
17. Akutsu Y, Kaneko K, Kodama Y et al (2011) Iodine-123-mibg imaging for predicting the development of atrial fibrillation. JACC Cardiovasc Imaging 4:78–86
18. Cohen-Solal A, Esanu Y, Logeart D et al (1999) Cardiac metaiodobenzylguanidine uptake in patients with moderate chronic heart failure: relationship with peak oxygen uptake and prognosis. J Am Coll Cardiol 33:759–766
19. Wakabayashi T, Nakata T, Hashimoto A et al (2001) Assessment of underlying etiology and cardiac sympathetic innervation to identify patients at high risk of cardiac death. J Nucl Med 42:1757–1767
20. Agostini D, Verberne HJ, Burchert W et al (2008) I-123- MIBG myocardial imaging for assessment of risk for a major cardiac event in heart failure patients: insights from a retrospective European multicenter study. Eur J Nucl Med Mol Imaging 35:535–546
21. Tamaki S, Yamada T, Okuyama Y et al (2009) Cardiac iodine-123 metaiodobenzylgunidine I-123-MIBG predicts sudden cardiac death independently of left ventricular ejection fraction in patients with

chronic heart failure and left ventricular systolic dysfunction. J Am Coll Cardiol 53:426–435
22. Gerson MC, Caldwell JH, Ananthasubramaniam K et al (2011) Influence of diabetes mellitus on prognostic utility of imaging of myocardial sympathetic innervation in heart failure patients. Circ Cardiovasc Imaging 4:87–93
23. Kuramoto Y, Yamada T, Tamaki S et al (2011) Usefulness of cardiac iodine-123 MIBG imaging to improve prognostic power of seattle heart failure model in patients with chronic heart failure. Am J Cardiol 107:1185–1190
24. Ketchum ES, Jacobson AF, Caldwell JL et al (2012) Selective improvement in seattle heart failure model risk stratification using iodine-123 meta-iodobenzylguanidine imaging. J Nucl Cardiol (in press)
25. Verberne HJ, Verschure DO, Veltman CE et al (2012) For what endpoint does myocardial $^{123}$I-MIBG scintigraphy have the greatest prognostic value in patients with heart failure? results of a pooled individual patient data meta-analysis. Eur Heart J (in press)
26. Gerson MC, Craft LL, McGuire N, Suresh DP, Abraham WT, Wagoner LE (2002) Carvedilol improves left ventricular function in heart failure patients with idiopathic dilated cardiomyopathy and a wide range of sympathetic nervous system function as measured by iodine123 metaiodobenzylguanidine. J Nucl Cardiol 19:608–615
27. Kasama S, Toyama T, Sumino H et al (2008) Prognostic value of serial cardiac $^{123}$I-MIBG imaging in patients with stabilized chronic heart failure and reduced left ventricular ejection fraction. J Nucl Med 49:907–914
28. Akashi YJ, Nakazawa K, Sakakibara M, Miyake F, Musha H, Sasaka K (2004) $^{123}$I-MIBG myocardial scintigraphy in patients with takostubo cardiomyopathy. J Nucl Med 45:1121–1127
29. Hakusui S, Yasuda T, Yanagi T et al (1994) A radiological analysis of heart sympathetic functions with meta-[$^{123}$I] iodobenzylguanidine in neurological patients with autonomic failure. J Auton Nerv Syst 49:81–84
30. Nakajima K, Yoshita M, Matsuo S, Taki J, Kinuya S (2008) Iodine-123-MIBG sympathetic imaging in Lewy-body diseases and related movement disorders. Q J Nucl Med Mol Imaging 52:378–387
31. Wakabayashi K, Takahashi H (1997) Neuropathology of autonomic nervous system in Parkinson's disease. Eur Neurol 38(Suppl 2):2–7
32. Iwanaga K, Wakabayashi K, Yoshimoto M et al (1999) Lewy body-type degeneration in cardiac plexus in Parkinson's and incidental Lewy body diseases. Neurology 52:1269–1271
33. McKeith IG (2006) Consensus guidelines for the clinical and pathologic diagnosis of dementia with Lewy bodies (DLB): report of the consortium on DLB international workshop. J Alzheimers Dis 9:417–423
34. Treglia G, Cason E, Giordano A (2012) Diagnostic performance of myocardial innervation imaging using MIBG scintigraphy in differential diagnosis between dementia with Lewy bodies and other dementias: a systematic review and a meta-analysis. J Neuroimaging 22:111–117
35. Estorch M, Camacho V, Paredes P et al (2008) Cardiac $^{123}$I-metaiodobenzylguanidine imaging allows early identification of dementia with Lewy bodies during life. Eur J Nucl Med Mol Imaging 35:1636–1641
36. Yoshita M, Taki J, Yokoyama K et al (2006) Value of $^{123}$I-MIBG radioactivity in the differential diagnosis of DLB from AD. Neurology 66:1850–1854
37. Nakajima K, Okuda K, Matsuo S et al (2012) Standardization of metaiodobenzylguanidine heart to mediastinum ratio using a calibration phantom: effects of correction on normal databases and a multicentre study. Eur J Nucl Med Mol Imaging 39:113–119
38. King AE, Mintz J, Royall DR (2011) Meta-analysis of $^{123}$I-MIBG cardiac scintigraphy for the diagnosis of Lewy body-related disorders. Mov Disord 26:1218–1224
39. Hanyu H, Shimizu S, Hirao K et al (2006) Comparative value of brain perfusion SPECT and [$^{123}$I]MIBG myocardial scintigraphy in distinguishing between dementia with Lewy bodies and Alzheimer's disease. Eur J Nucl Med Mol Imaging 33:248–253